Performance of bEPIC Through the 2024 M 7.0 Mendocino Earthquake Sequence

OPEN ACCESS

Amy Williamson[*1], Angela Lux[1], and Richard M. Allen[1]

Abstract

On 5 December 2024, an **M** 7.0 earthquake ruptured offshore of Cape Mendocino, California, generating felt shaking along the coast and prompting the issuance of earthquake early warning alerts and a tsunami warning. Contemporaneous to the earthquake sequence, bEPIC, an update to the ShakeAlert early warning algorithm Earthquake Point-source Integrated Code (EPIC), was undergoing development tests in real-time. The observed earthquake sequence provided a rich dataset of earthquakes in which we could test the performance of bEPIC. bEPIC improved epicenter estimates with an average 29.7 km reduction in location error compared to EPIC solutions for matched events. The improvement in location also improved per event magnitude estimates. Although EPIC on average overestimated the maximum magnitude of the earthquakes in the sequence by 0.37 magnitude units, bEPIC more closely aligned with our ground-truth catalog with a much lower overestimate of only 0.05 magnitude units. Despite including more information in the grid-search algorithm, bEPIC did not increase the average time to the first alert. The improvements in the accuracy of the earthquake parameters ultimately improve the accuracy of potential alerting polygons, which are related to the solved location and magnitude. These promising results indicate that improved accuracy with no cost to timeliness can be achieved for offshore earthquakes in northern California through the incorporation of bEPIC in early warning operating procedures.

Introduction

On 5 December 2024, an **M** 7.0 earthquake ruptured offshore of Cape Mendocino, California. The earthquake ruptured on the right-lateral Mendocino transform fault. The eastern terminus of the transform is the Mendocino Triple Junction, a complex tectonic environment accommodating motion between the Pacific, Gorda, and North American plates. Numerous large earthquakes have ruptured offshore of Cape Mendocino over contemporary seismic history. Earthquakes commonly rupture either on the transform or on other proximal faults within the nearby subducting slab or the Gorda transform system (Rollins and Stein, 2010). Recently the 20 December 2022 either algorithm to generate their first solution 6.4 Ferndale earthquake ruptured north of the transform system. This earthquake was preceded by one year by the 20 December 2021 **M** 6.0 doublet (Yeck *et al.*, 2023; Hellweg *et al.*, 2024). All three of these

recent large earthquakes ruptured within 50 km of the 2024 earthquake.

To date, over 500 aftershocks have been detected, mostly east (landward) of the mainshock (Fig. 1). Most aftershocks have been small, offshore, and therefore not felt along the coastline. The largest aftershock to date is an **M** 5.3 rupturing west of the mainshock on 14 December 2024. These aftershocks were detected through the dense seismic network of regional stations. During the time of the sequence, 116 stations were located

1. UC Berkeley Seismological Laboratory, University of California, Berkeley, Berkeley, California, U.S.A., https://orcid.org/0000-0002-3767-6018 (AL); https://orcid.org/0000-0003-4293-9772 (RMA)

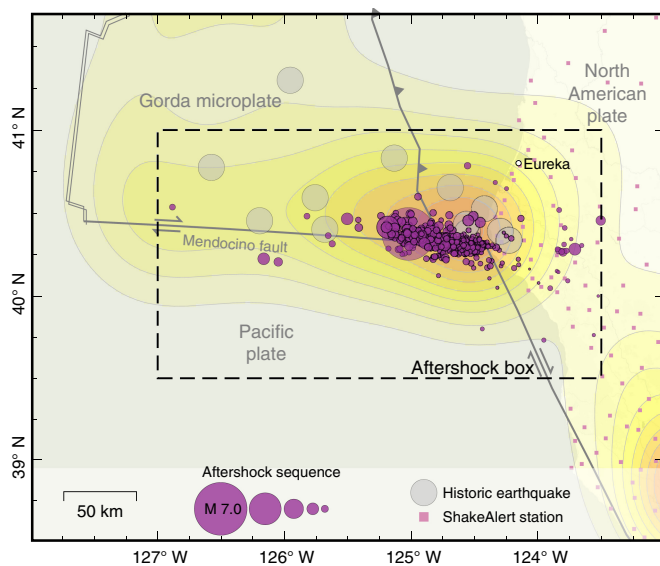*Corresponding author: amy.williamson@berkeley.edu

Figure 1. Map of the study area. The purple circles show seismicity from the time of the **M** 7.0 mainshock through 9 January 2025 inside the defined aftershock region (black dashed line). The purple circles are scaled to the reported Comprehensive Earthquake Catalog (ComCat) magnitude. The gray circles, not scaled, indicate epicenters of **M** 6.0 and greater earthquakes from 1992 to December 2024. The pink small squares on land indicate the location of ShakeAlert stations. The yellow-to-orange shading shows the relative weight used in bEPIC's prior seismicity kernel. The darker shading indicates more prior seismicity and a larger weight.

within 200 km of the mainshock epicenter. Because of the lack of local ocean-bottom sensors, these stations are the first instruments to detect the oncoming seismic waves.

The mainshock of the Offshore Cape Mendocino sequence was large enough to activate the ShakeAlert system. Shake Alert is an earthquake early warning (EEW) system operating in California, Oregon, and Washington (Kohler *et al.*, 2020). ShakeAlert takes information from up to three participating EEW algorithms: the Earthquake Point-source Integrated Code (EPIC; Chung *et al.*, 2019), the Finite-fault rupture detector (FinDer; Böse *et al.*, 2015, 2018), and a GNSS peak ground displacement algorithm: Geodetic First Approximation of Size and Time (GFAST-PGD; Murray *et al.*, 2023). During the mainshock, both EPIC and FinDer produced earthquake parameter estimates that when combined were used to issue a first alert 15.1 s after origin time. Because of the large magnitude of the earthquake, EEW alerts were issued to affected communities through a wireless emergency alert (WEA) and third-party smartphone applications like MyShake (Strauss *et al.*, 2020; Patel and Allen, 2022).

The region surrounding the earthquake sequence was previously identified as an area where EPIC commonly

mischaracterizes earthquakes (Kohler *et al.*, 2020). EPIC mislocates the epicenter of offshore earthquakes in northern California west (further seaward) of their true location. The error from poor location estimates propagates into an error in the estimated magnitude and expected ground motions. Ultimately these errors may cause the communities to receive an untimely alert, or in some cases where the location estimate is too far seaward, no alert is issued at all.

To improve EEW location estimates for earthquakes offshore and at the edge of seismic networks, Williamson *et al.* (2023) proposed a modification of the EPIC location algorithm coined bEPIC. This modification combines a weighting scheme based on regional prior seismicity with EPIC's 2D grid-search algorithm. Initial tests completed in Williamson *et al.* (2023) showed a large reduction in epicentral location errors for earthquakes originating offshore of northern California, among other regions. After completion of these preliminary tests, bEPIC was modified to fit within the current EEW architecture in ShakeAlert and has been running in real-time alongside EPIC, on a development machine where it is not permitted to contribute to public alerts. As such, bEPIC was operating in real-time throughout the earthquake sequence, providing a rich dataset of detections for which to compare with EPIC. This comparison allows us to identify differences in the number of detected events, location and magnitude estimates, and additional real-time information such as the timing of the first alerts issued.

In this study, we compare bEPIC's ability to detect and locate offshore earthquakes from the **M** 7.0 earthquake sequence against the EPIC solution. We focus on location accuracy, rates of earthquake detection, downstream parameter improvements to the magnitude, and first alert timing. We also highlight how utilizing bEPIC improves the potential alerting footprint. The performance during this sequence can act as an example of expected performance for future large earthquakes within this seismically active region.

Data and Methods
Parameter estimates within EPIC and bEPIC
EPIC is composed of multiple algorithms that, as a whole, ingest processed seismic data from a network of ShakeAlert stations and output an estimate of the earthquake epicenter, magnitude, and origin time. These algorithms include (1) a station associator, which takes and groups triggered stations based on their *P*-wave trigger time and distance; (2) the location algorithm, which takes these grouped stations and determines an epicentral location that best fits the *P*-wave

trigger times using a 1D velocity model; and (3) a magnitude algorithm that uses the (just calculated) epicenter, station distances, observed peak displacement measurements, and an empirical scaling relationship. These algorithms work in series, updating estimates as new station triggers are associated, or new data are acquired from already associated stations. EPIC's output, a time series of parameter estimates, is ingested into a different set of ShakeAlert algorithms that merges EPIC's solutions with the solutions from other participating algorithms like FinDER and/or GFAST-PGD. For a more detailed description of the entire ShakeAlert algorithm architecture including additional information about the processing and parameter decisions made in EPIC, please refer to Chung *et al.* (2019) and Lux *et al.* (2024).

EPIC's location algorithm employs a 2D grid search. The epicenter is chosen as the grid node that has the lowest root mean square misfit between observed *P*-wave trigger times and a model of the expected trigger times using a 1D velocity model. A downside of the current EPIC algorithm is the non-uniqueness of location estimates that occur along the edge of the seismic network, particularly offshore. This is typically due to the one-sidedness of the station geometry along the coastline. The result is a best location that is drawn from a grid that has many areas with equal or near equally low misfit. In the case of the Mendocino region, EPIC has mislocated earthquakes hundreds of kilometers offshore and away from the correct location.

bEPIC modifies the location algorithm while maintaining the rest of the current EPIC architecture and source parameters. bEPIC uses the same *P*-wave trigger times as a dataset but combines the misfit per grid node with a grid weighting based on a 2D kernel density estimate of past seismicity. The inclusion of this prior seismicity kernel's impact is strongest in cases where the grid solution is nonunique. In these cases, the best epicenter location is the one with the combination of lowest misfit and highest prior seismicity. In initial tests completed in Williamson *et al.* (2023), bEPIC substantially lowered location errors in offshore and edge-of-network regions. For additional details describing how bEPIC is formulated and specific model parameters used, please refer to Williamson *et al.* (2023).

In 2024, bEPIC was reformatted to operate in real-time, recreating the environment used in the ShakeAlert production system including the use of data from stations currently employed in ShakeAlert. Since September 2024, bEPIC has been operating on a development machine alongside EPIC. Although not permitted to contribute to ShakeAlert public alerts, bEPIC detects and estimates earthquake parameters in real-time, ingesting the same data streams as other algorithms within ShakeAlert. These data are saved in daily log files and can be reviewed by analysts.

Real-time dataset

The Offshore Cape Mendocino mainshock and aftershock sequence were detected by EPIC through the broader ShakeAlert solution, and bEPIC through a real-time but independent algorithm in development. This study utilizes the EPIC and bEPIC daily log files produced throughout the earthquake sequence. We generate two catalogs in this study. The first catalog includes every earthquake detected and logged from EPIC inside our designated aftershock area (shown in Fig. 1). The second catalog includes every earthquake detected and logged from bEPIC over the same region. The EPIC and bEPIC catalogs, while ingesting the same data, have the potential to detect different numbers of earthquakes. For example, if an earthquake epicenter is located too far from the seismic network (>200 km), it is rejected. Because of the potential for poor location estimates, this can happen in the real-time characterization from one algorithm and not the other. In addition, the exact timing and processing of data packets from associated seismic stations may vary slightly between different ShakeAlert machines (Cochran *et al.*, 2018). This can lead to small differences between different station detection times that while minor, can cause some differences between the two catalogs.

The earthquakes detected by both EPIC and bEPIC are retrospectively matched against the Advanced National Seismic System Comprehensive Catalog (ComCat; U.S. Geological Survey [USGS], Earthquake Hazards Program, 2017). To measure performance, we hold the coordinates of any matched ComCat earthquake as the true epicenter. We compare the resulting EPIC and bEPIC estimated magnitudes against the ComCat preferred magnitude for each event, rather than use one type of magnitude (i.e., local magnitude). This allows us to remain consistent with performance analysis in previous ShakeAlert algorithm-focused studies (Böse *et al.*, 2023).

Results and Discussion

From 5 December 2024 to 9 January 2025, 524 earthquakes located inside the Mendocino sequence area were cataloged through the ComCat database. These events include the mainshock **M** 7.0, and the largest aftershock in the sequence (**M** 5.3) in addition to hundreds of smaller events. The earthquakes detected by both EPIC and bEPIC are shown in Figure 2 as detections as a function of time since the mainshock and in
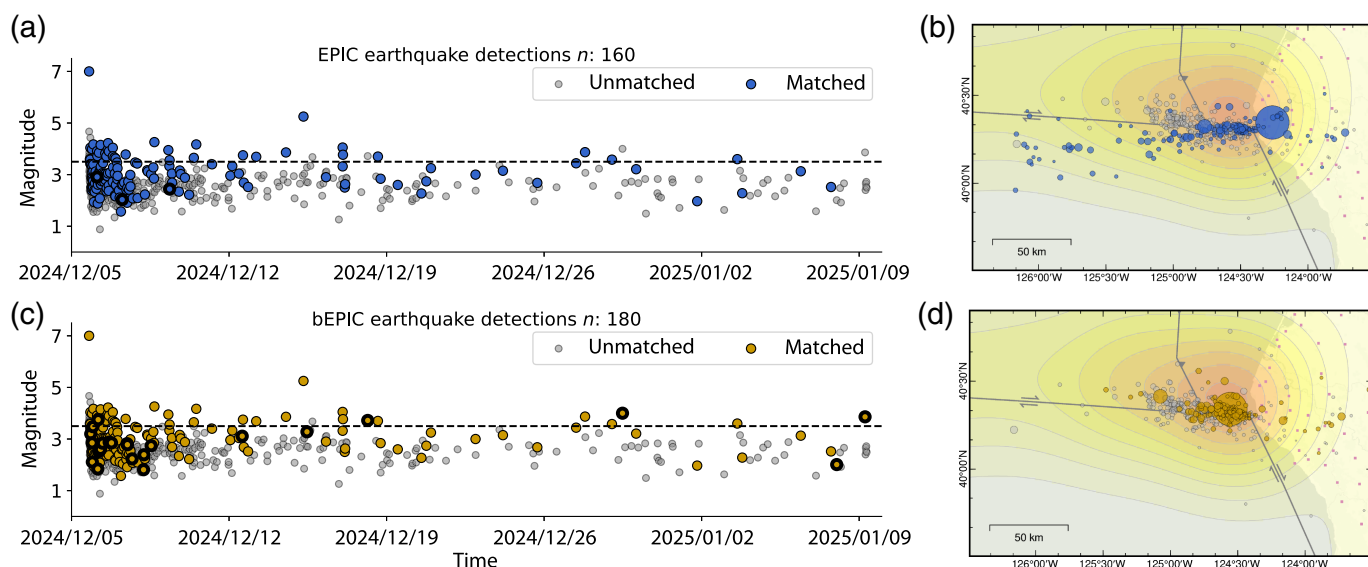
Figure 2. Earthquake Point-source Integrated Code (EPIC) and bEPIC detections made in real-time compared to the Advanced National Seismic System (ANSS) ComCat catalog. Detected earthquakes for EPIC and bEPIC are colored in blue and yellow, respectively. Earthquakes that were not detected by each respective algorithm are colored in gray. (a) Time series of EPIC detections starting at the time of the mainshock. (b) Map view of EPIC locations at the time of minimum location error. (c) Time series of bEPIC detections starting at the time of the mainshock. (d) Map view of the bEPIC locations at the time of minimum location error. The bolded circles in panels (a) and (c) are earthquakes that were only detected by one of the two algorithms, either EPIC or bEPIC. The black dashed line marks **M** 3.5. The yellow-to-orange shading in panels (b) and (d) shows the relative prior weighting with the same scaling as in Figure 1.
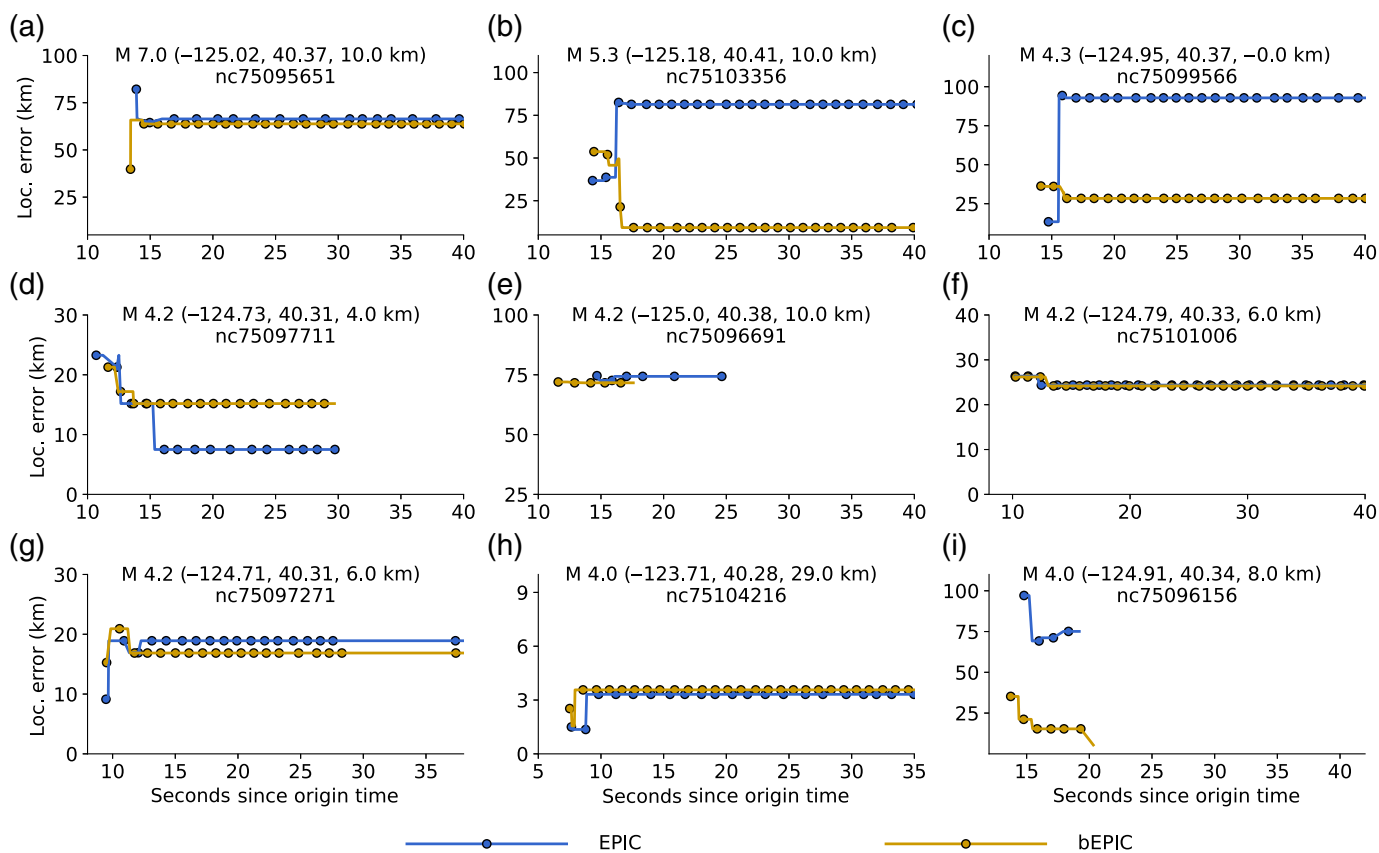
map view. Mapped locations for detected events from EPIC and bEPIC use the location at the point with the lowest location error. During this time, EPIC detected 160 earthquakes and bEPIC detected 180 earthquakes. bEPIC detected 23 events that were missed by EPIC. Conversely, EPIC detected three earthquakes that were missed by bEPIC. At all magnitude ranges, EPIC and bEPIC both detected a common set of 157 earthquakes with a magnitude ranging from **M** 1.6 to 7.0.

As EPIC and its update, bEPIC, relay information for use in EEW, we are most interested in their performance at alerting magnitude thresholds. Within the ShakeAlert system, alerts are disseminated through WEA systems for **M** 5.0 and greater earthquakes. Third-party smartphone applications like MyShake alert at a lower **M** 4.5 threshold. Because of the relative scarcity of **M** 4.5 and greater earthquakes in the aftershock sequence, we lower this threshold slightly and focus on each algorithm's ability to detect earthquakes at **M** 3.5 and greater. Of the 51 earthquakes that are **M** 3.5 or greater, EPIC detected 36 and bEPIC detected 40. Among the 11 **M** 3.5+ earthquakes that both algorithms missed, 10 occurred in the first five hours following the mainshock. Because of the large number of earthquakes occurring in a short period and small geographic area, we expect a lower detection rate. Outside of the first hours, bEPIC detected three additional **M** 3.5+ earthquakes that EPIC missed.

The detection and characterization of an earthquake through EPIC and bEPIC created a dynamic set of location and magnitude estimates because new stations trigger and are associated with the event with increasing time. The time-series evolution

of epicentral location errors for the mainshock and the eight largest aftershocks is shown in Figure 3. Location errors are calculated as the great circle distance in kilometers between the algorithm epicenter and the final ComCat epicenter. Source depth is not included in the location error analysis because EPIC assumes a source depth of 8 km. This depth is based on a mean crustal earthquake depth in California and is found to be an efficient way to limit parameters in the location grid search (Brown *et al.*, 2011). The mean depth of earthquakes within this aftershock sequence as reported through ComCat is 10.6 km.

bEPIC generates lower location errors over the solution time series for eight of the nine largest earthquakes shown in Figure 3. In the case where EPIC performs better than bEPIC (Fig. 3d), the location of both algorithms is similar with a location error of 8 and 15 km between EPIC and bEPIC, respectively. Noteworthy is the improvement in location estimates

Figure 3. Epicentral location time-series estimates from EPIC (blue) and bEPIC (yellow) for (a) the **M** 7.0 mainshock and (b–i) the eight largest matched aftershocks. Location error is calculated epicentral distance between the algorithm estimate and the non-real-time Comprehensive Catalog (ComCat) location.

for the two largest aftershocks, Figure 3b,c. In both estimates, EPIC mislocated the earthquakes over 75 km from their correct locations.
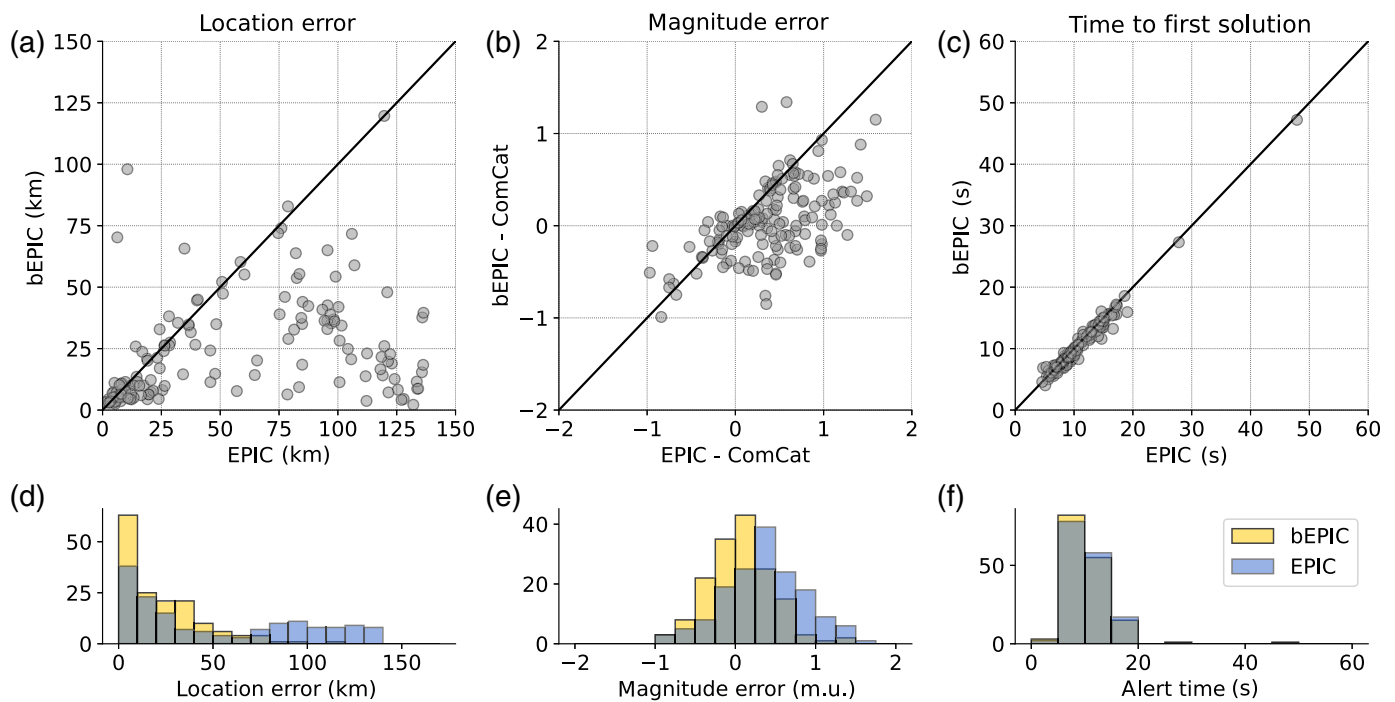
Although EPIC and bEPIC behave somewhat differently for many of the events in the aftershock sequence, both algorithms had very similar solutions for the mainshock after the first estimated location (Fig. 3a). This is because both EPIC and bEPIC utilized the same station that triggered a few seconds before the mainshock on a possible small foreshock. Because this early trigger was erroneously associated with the mainshock, the attempt to fit both the correct and incorrect triggers led to a subpar location with errors close to 70 km. Neither EPIC nor bEPIC have a mechanism in place to judge the likelihood that a trigger is correct, and all triggers associated are always treated equally in the calculation of the location misfit. The inclusion of the prior does not largely affect the solution in cases where location is considered well-constrained, albeit with poor-quality input data.

Figure 4 shows the maximum location error, maximum magnitude error, and time to first alert for all EPIC- and bEPIC-matched earthquakes. The maximum location error is taken at the point in the solution time series when the distance between the algorithm epicenter and ComCat epicenter is greatest. The average of the maximum location estimates within EPIC is 53 km and within bEPIC is 23 km. The distribution of maximum location errors within EPIC (Fig. 4d) shows a weakly bimodal distribution with a concentration of solutions with location errors under 10 km and a second set of solutions with errors closer to 90 km. bEPIC does not share this same distribution and does not have a concentration of high location error solutions. Furthermore, while bEPIC does produce some large location error solutions, here defined as a location error above 50 km, in all but three solutions, EPIC produced an even larger error for the same events. Although this means that there is still additional improvement possible, the location errors found in bEPIC are an improvement from the current system.

Although bEPIC only modifies the location algorithm, poor location estimates often lead to poor magnitude estimates as

Figure 4. EPIC and bEPIC matched dataset performance. (a) Comparison of bEPIC and EPIC location errors, in kilometers. 1:1 line drawn in black. (b) A comparison of magnitude residuals. Residual is defined as the difference between the tested algorithm (EPIC or bEPIC) and the ComCat final magnitude. (c) Comparison of time, in seconds, to a first solution. Histograms of the location error, magnitude error, and solution times from (a) to (c), are displayed in (d–f). The yellow histogram shows the bEPIC distribution for each performance metric. The blue histogram shows the EPIC distribution for the same metrics.

the two processes are connected. Magnitudes in EPIC are estimated using the now-known station epicentral distance, a measure of the peak displacement at each station component, and a pre-derived empirical scaling relationship (Kuyuk and Allen, 2013; Chung et al., 2019). We therefore investigate the quality of the magnitude estimates of this sequence between bEPIC and EPIC and present the results in Figure 4b. Here, we focus on the magnitude performance at the point in the solution time series when the magnitude is largest. Presented in Figure 4b is a comparison of the difference, in magnitude units, between both bEPIC against the ComCat preferred magnitude and EPIC against the same ComCat magnitude. In a perfect solution, the magnitude residual between either algorithm and the ComCat magnitude would be zero, indicating perfect agreement between the two datasets. EPIC, on average, overestimates the magnitude by 0.37 magnitude units (m.u.). bEPIC on average overestimates the magnitude by only 0.05 m.u. It should be noted that there is a large spread in magnitude residuals for both bEPIC and EPIC. The good agreement in the magnitude estimates of bEPIC is likely directly related to the improvement in the estimate of the station epicentral distance.

Because bEPIC has been running in real-time, an additional tested feature is the time that it takes either algorithm to generate their first solution. This time includes the time for seismic waves to arrive at nearby stations, data telemetry,

and computation time. In addition, solutions must pass quality control metrics to be published. This includes associating a minimum of four different stations and having at least one station located within 200 km of the estimated epicenter. For all events that have both an EPIC and a bEPIC solution, bEPIC had an average first alert time of 10.56 s to EPIC's 10.96 s. This means that while similar, bEPIC is on average 0.4 s faster. Although promising, we also note that because bEPIC and EPIC run on separate machines, there may also be differences in computational load which can affect overall timing. We therefore treat these timing results as an indication that bEPIC does not slow the system, rather than focus on the sub-second accuracy.

The ultimate goal of any potential improvements to the EEW system is to provide more informed and accurate alerts to those who may experience damaging shaking. Improvements to the estimate of the earthquake's epicenter have a cascading effect
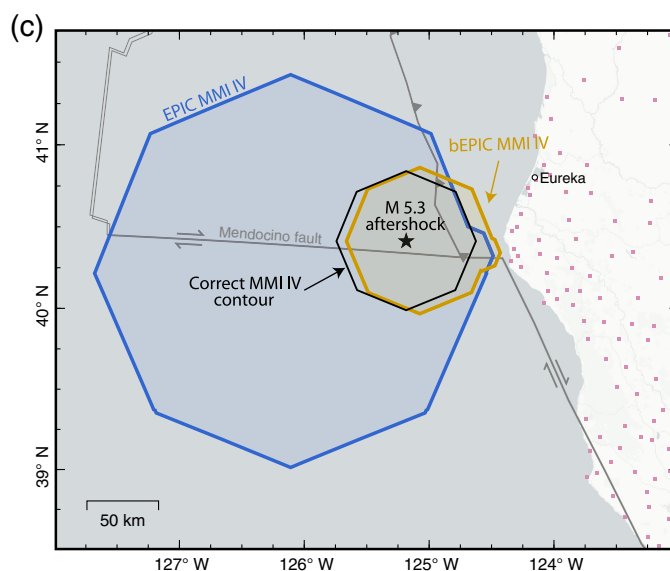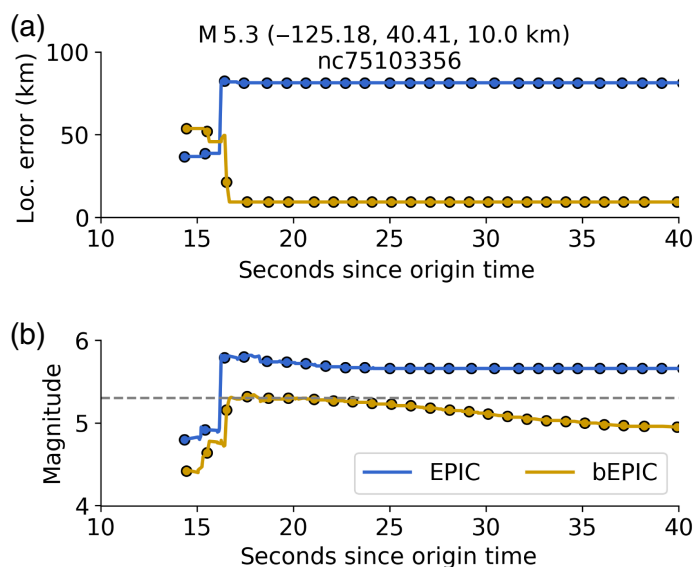
Figure 5. Performance and alerting contours for the largest aftershock (**M** 5.3). (a) Epicenter location error for EPIC (blue) and bEPIC (yellow) in kilometers. (b) Magnitude estimates from EPIC and bEPIC compared with the ComCat magnitude (gray dashed line). (c) Comparison of the expected modified Mercalli intensity (MMI) 4 alerting contour between EPIC and bEPIC based on the alert location and magnitude histories from panels (a) and (b). This is compared with the expected alerting contour based on the static ComCat location and magnitude (black polygon). The pink squares are stations included in the ShakeAlert network.

on the rest of the solution processes. With an improved epicenter, a more accurate magnitude can be calculated. These two pieces of information are used as the input into ground-motion models that are used to calculate estimated shaking. As such, they govern the size of the expected alerting area, defined in ShakeAlert as an eight-sided polygon (Thakoor *et al.*, 2019; Kohler *et al.*, 2020). With the increasing magnitude and finite-source information from FinDer, the eight-sided polygon can extend into a more complex shape. The size of the polygon represents the expected distance of different levels of modified Mercalli intensity (MMI) shaking.

bEPIC's improvement in location and magnitude translates to potential alerting regions that more closely align with what would be expected based on the ComCat epicenter and magnitude. Illustrated in Figure 5 is the total alerting extent of both EPIC and bEPIC compared to the expected alert area for the largest aftershock in the Mendocino sequence, an **M** 5.3 earthquake that occurred 10 days after the mainshock. Although bEPIC's total alerting area is similar to the "correct" polygon, EPIC's alerting area is significantly larger due to the large location and magnitude misestimate. Note the full alerting polygons for both EPIC and bEPIC are not perfect octagons, but instead are a combination of all polygons generated over the alerting time series. Because of the similarities in the location time series from both EPIC and bEPIC, visible in Figure 3a, the alerting areas for the **M** 7.0 mainshock are very similar (Fig. S1, available in the supplemental material to this article).

The region offshore of northern California has consistently generated **M** 6 and greater earthquakes, with 15 occurrences

over the past 35 yr alone. Therefore, it is important to have EEW algorithms that are tuned to detect and characterize these sorts of earthquakes. Because of the one-sidedness of the seismic network and the lack of offshore seismic instrumentation, bEPIC helps fill an information and data gap. The improvements shown in bEPIC during the aftershock sequence provide promise for increased detection and improved alerting zones during future earthquakes in this region. High-quality real-time earthquake information is useful not only for immediate use in EEW alerts, but can also provide situational awareness during secondary hazards such as tsunamis (Williamson and Allen, 2023).

Conclusion

The **M** 7.0 Offshore Cape Mendocino earthquake and aftershock sequence was the first large-scale test of bEPIC while the algorithm has been running in real-time on development servers. bEPIC ingests the same real-time data streams for the same stations as EPIC, generating solutions that stop short of

sending out alerts. What we discovered when analyzing the aftershock sequence using both algorithms is that bEPIC is effective in detecting more earthquakes, including more **M** 3.5 and larger earthquakes than EPIC. In addition, the location estimates provided by bEPIC are on average 30 km lower at the point of maximum error. This improvement in location translates to an improvement in the magnitude estimate, with the maximum bEPIC magnitude estimate closely aligned with the ComCat magnitude. Finally, these improvements do not impact or slow down the algorithm, providing first solution times that are 0.4 s faster than EPIC. These improvements result in a more accurate representation of the alerting polygon, as illustrated in Figure 5 for the largest aftershock in the sequence. These real-time results indicate that the implementation of bEPIC as an operational tool would improve the accuracy of offshore earthquakes and should be adopted for use in EEW.

Data and Resources

Earthquake Point-source Integrated Code (EPIC) and bEPIC catalogs are available as a supplemental dataset. These catalogs were matched to earthquakes within the Advanced National Seismic System (ANSS) Comprehensive Earthquake Catalog (ComCat) through a post-event query through the ComCat website https://earthquake.usgs.gov/data/comcat/ (last accessed January 2025). Some plots were made using PyGMT (https://zenodo.org/record/6702566; Wessel *et al.*, 2019; Uieda *et al.*, 2022). The source code for bEPIC is available through GitHub: https://github.com/amy-l-williamson/bEPIC. All websites were last accessed in March 2025.

Declaration of Competing Interests

The authors acknowledge that there are no conflicts of interest recorded.

Acknowledgments

References

Böse, M., J. Andrews, R. Hartog, and C. Felizardo (2023). Performance and next-generation development of the finite-fault rupture detector (FinDer) within the United States West Coast ShakeAlert warning system, *Bull. Seismol. Soc. Am.* **113,** no. 2, 648–663, doi: 10.1785/0120220183.

Böse, M., C. Felizardo, and T. H. Heaton (2015). Finite-fault rupture detector (FinDer): Going real-time in Californian ShakeAlert warning system, *Seismol. Res. Lett.* **86,** no. 6, 1692–1704.

Böse, M., D. E. Smith, C. Felizardo, M. A. Meier, T. H. Heaton, and J. F. Clinton (2018). FinDer v. 2: Improved real-time ground-motion predictions for M2–M9 with seismic finite-source characterization, *Geophys. J. Int.* **212,** no. 1, 725–742.

Brown, H. M., R. M. Allen, M. Hellweg, O. Khainovski, D. Neuhauser, and A. Souf (2011). Development of the ElarmS methodology for earthquake early warning: Realtime application in California and offline testing in Japan, *Soil Dynam. Earthq. Eng.* **31,** no. 2, 188–200, doi: 10.1016/j.soildyn.2010.03.008.

Cochran, E. S., M. D. Kohler, D. D. Given, S. Guiwits, J. Andrews, M. A. Meier, M. Ahmad, I. Henson, R. Hartog, and D. Smith (2018). Earthquake early warning ShakeAlert system: Testing and certification platform, *Seismol. Res. Lett.* **89,** no. 1, 108–117, doi: 10.1785/0220170138.

Chung, A. I., I. Henson, and R. M. Allen (2019). Optimizing earthquake early warning performance: ElarmS-3, *Seismol. Res. Lett.* **90,** no. 2A, 727–743, doi: 10.1785/0220180192.

Hellweg, M., D. S. Dreger, A. Lomax, R. C. McPherson, and L. Dengler (2024). The 2021 and 2022 North Coast California earthquake sequences and fault complexity in the vicinity of the Mendocino triple junction, *Bull. Seismol. Soc. Am.* doi: 10.1785/0120240023.

Kohler, M. D., D. E. Smith, J. Andrews, A. I. Chung, R. Hartog, I. Henson, D. D. Given, R. de Groot, and S. Guiwits (2020). Earthquake early warning ShakeAlert 2.0: Public rollout, *Seismol. Res. Lett.* **91,** no. 3, 1763–1775, doi: 10.1785/0220190245.

Kuyuk, H. S., and R. M. Allen (2013). A global approach to provide magnitude estimates for earthquake early warning alerts, *Geophys. Res. Lett.* **40,** no. 24, 6329–6333, doi: 10.1002/2013GL058580.

Lux, A. I., D. Smith, M. Böse, J. J. McGuire, J. K. Saunders, M. Huynh, I. Stubailo, J. Andrews, G. Lotto, B. Crowell, *et al.* (2024). Status and performance of the ShakeAlert earthquake early warning system: 2019–2023, *Bull. Seismol. Soc. Am.* **114,** no. 6, 3041–3062, doi: 10.1785/0120230259.

Murray, J. R., B. W. Crowell, M. H. Murray, C. W. Ulberg, J. J. McGuire, M. A. Aranha, and M. T. Hagerty (2023). Incorporation of real-time earthquake magnitudes estimated via peak ground displacement scaling in the ShakeAlert earthquake early warning system, *Bull. Seismol. Soc. Am.* **113,** no. 3, 1286–1310, doi: 10.1785/0120220181.

Patel, S. C., and R. M. Allen (2022). The MyShake App: User experience of early warning delivery and earthquake shaking, *Seismol. Soc. Am.* **93,** no. 6, 3324–3336.

Rollins, J. C., and R. S. Stein (2010). Coulomb stress interactions among M≥ 5.9 earthquakes in the Gorda deformation zone and on the Mendocino Fault Zone, Cascadia subduction zone, and northern San Andreas Fault, *J. Geophys. Res.* **115,** no. B12, doi: 10.1029/2009JB007117.

Strauss, J. A., Q. Kong, S. Pothan, S. Thompson, R. F. Mejia, S. Allen, S. Patel, and R. M. Allen (2020). MyShake citizen seismologists help

launch dual-use seismic network in California, *Front. Commun.* **5,** 32, doi: 10.3389/fcomm.2020.00032.

Thakoor, K., J. Andrews, E. Hauksson, and T. Heaton (2019). From earthquake source parameters to ground-motion warnings near you: The ShakeAlert earthquake information to ground-motion (eqInfo2GM) method, *Seismol. Res. Lett.* **90,** no. 3, 1243–1257.

Uieda, L., D. Tian, W. J. Leong, M. Jones, W. Schlitzer, M. Grund, L. Toney, J. Yao, Y. Magen, K. Materna, *et al.* (2022). PyGMT: A Python interface for the Generic Mapping Tools (v0.7.0), *Zenodo*, doi: 10.5281/zenodo.6702566.

U.S. Geological Survey (USGS), Earthquake Hazards Program (2017). Advanced national seismic system (ANSS) comprehensive catalog of earthquake events and products: Various, doi: 10.5066/F7MS3QZH.

Wessel, P., J. F. Luis, L. Uieda, R. Scharroo, F. Wobbe, W. H. Smith, and D. Tian (2019). The generic mapping tools version 6, *Geochem. Geophys. Geosys.* **20,** no. 11, 5556–5564.

Williamson, A., and R. M. Allen (2023). Improving efficacy of tsunami warnings along the west coast of the United States, *Pure Appl. Geophys.* **180,** no. 5, 1661–1678, doi: 10.1007/s00024-023-03277-z.

Williamson, A., A. Lux, and R. Allen (2023). Improving out of network earthquake locations using prior seismicity for use in earthquake early warning, *Bull. Seismol. Soc. Am.* **113,** no. 2, 664–675, doi: 10.1785/0120220159.

Yeck, W. L., D. R. Shelly, K. Z. Materna, D. E. Goldberg, and P. S. Earle (2023). Dense geophysical observations reveal a triggered, concurrent multi-fault rupture at the Mendocino Triple Junction, *Commun. Earth Environ.* **4,** no. 1, 94, doi: 10.1038/s43247-023-00752-2.